

Evaluation of manoeuvring coefficients of a self-propelled ship using a Blade Element Momentum propeller model coupled to a Reynolds averaged Navier Stokes flow solver

Alexander Phillips¹, Stephen R. Turnock¹, Maaten Furlong²
¹ School of Engineering Sciences, University of Southampton
² National Oceanography Centre, Southampton

Abstract

The use of an unsteady Computational Fluid Dynamic analysis of the manoeuvring performance of a self-propelled ship requires a large computational resource that restricts its use as part of a ship design process. A method is presented that significantly reduces computational cost by coupling a Blade Element Momentum Theory (BEMT) propeller model with the solution of the Reynolds Averaged Navier Stokes (RANS) equations. The approach allows the determination of manoeuvring coefficients for a self-propelled ship travelling straight ahead, at a drift angle and for differing rudder angles. The swept volume of the propeller is divided into discrete annuli for which the axial and tangential momentum changes of the fluid passing through the propeller are balanced with the blade element performance of each propeller section. Such an approach allows the interaction effects between hull, propeller and rudder to be captured. Results are presented for the fully appended model scale self propelled KVLCC2 hull form under going static rudder and static drift tests at a Reynolds number of 4.6×10^6 acting at the ship self propulsion point. All computations were carried out on a typical workstation using a hybrid finite volume mesh size of 2.1×10^6 elements. The computational uncertainty is typically 2-3% for side force and yaw moment.

Keywords: ship manoeuvring; self propulsion, CFD, validation, rudder-propeller interaction, self-propulsion

Nomenclature

| | |
|--------------|---|
| a | Axial flow factor |
| a' | Circumferential flow factor |
| B | Number of blades |
| B_T | Breadth of tank (m) |
| C | Blade chord (m) |
| C_D | Drag coefficient |
| C_L | Lift coefficient |
| D | Drag (N) |
| D_T | Depth of tank (m) |
| J | Advance coefficient |
| K | Goldstein correction factor |
| K_Q | Torque coefficient |
| K_T | Thrust coefficient |
| L | Lift (N) |
| L_{bp} | Length between perpendiculars (m) |
| n | Revolutions per second (s^{-1}) |
| N | Yaw moment (Nm) |
| P | Pressure (Pa) |
| Q | Torque (Nm) |
| R | Local radius (m) |
| R_k | Mesh refinement ratio |
| R | Resistance (N) |
| R_N | Reynolds number |
| R_x | Rudder x force (N) |
| R_y | Rudder y force (N) |
| t | Thrust deduction factor |
| T | Thrust (N) |
| u_i | Cartesian velocity components (m/s) |
| v | Ship sway velocity (m/s) |
| V_a | Propeller advance velocity (m/s) |
| w_t | nominal wake fraction |
| w_t' | Local nominal wake fraction |
| x_i | Cartesian co-ordinates (m) |
| X | Longitudinal force (N) |
| X/D | Longitudinal separation between rudder and propeller / propeller diameter |
| Y | Transverse force (N) |
| α | Incidence angle |
| ΔK_T | Increase in thrust coefficient due to presence of rudder |
| Δw_t | Increase in wake fraction due to the presence of the rudder |
| η | Efficiency |
| η_i | Ideal efficiency |
| ρ | Fluid density (kg/m^3) |
| ϕ | Hydrodynamic pitch angle (deg) |
| ψ | Undisturbed flow angle (deg) |
| Ω | Rotational velocity (s^{-1}) |

1 Introduction

The design assessment of the manoeuvring performance of a ship requires the evaluation of between 20 -30 derivative coefficients, ed. Comstock (1967). Such coefficients depend on the interaction between the forces and moments generated on the hull and rudder in the presence of the propeller, Molland and Turnock (2007). In order to accurately assess the forces acting on a manoeuvring vessel the interaction of the hull, propeller and rudder must be considered in the calculation of global forces. It is now possible to compute the interaction using an unsteady computational fluid dynamics (CFD) solver that models the full flow regime around the hull, propeller and rudder, ITTC, (2008). However, the necessary time step and mesh refinement, which are driven primarily by the need to capture the flow field around the propeller, results in a very large computational cost. The method proposed in this paper makes use of the flow integrating effect of the propeller which generates an accelerated and swirled onset flow onto the rudder while the rudder acts to block and divert the flow through the propeller, Turnock(1993). As long as the radial variation in axial and tangential momentum (including hull and rudder interaction effects) generated by the propeller are included, then the influence of the unsteady propeller flow can be removed and ‘steady’ calculations performed to evaluate the manoeuvring coefficients.

Table 1 presents the hierarchy of numerical methods for modelling propellers ranging in complexity and accuracy, Bertram (2000), Breslin and Anderson (1994). The actuator disc model based on momentum theory was implemented within a Reynolds Averaged Navier Stokes (RANS) simulation of the flow about a hull by Schetz and Favin(1977). Momentum theory can be adapted to run in conjunction with a RANS simulation where the predicted thrust and torque are implemented in the RANS simulation as a series of momentum sources distributed over the propeller disc.

Table 1: Numerical methods for modelling propellers

| Method | Description |
|---------------------------------|--|
| Momentum Theory | The propeller is modelled as an actuator disc over which there is a instantaneous pressure change, resulting in a thrust acting at the disc. The thrust, torque and delivered power are attributed to changes in the fluid velocity within the slipstream surrounding the disc, Rankine(1865), Froude (1889), and Froude (1911). |
| Blade Element Theory | The forces and moments acting on the blade are derived from a number of independent slices represented as a 2-D aerofoils at an angle of attack to the fluid flow. Lift and drag information for the slices must be provided <i>a priori</i> and the induced velocities in the fluid due to the action of the propeller are not accounted for, Froude (1878) . |
| Blade Element Momentum Theory | By combining Momentum theory with blade element theory, O'brian (1969), the induced velocity field can be found around the 2D-sections. Corrections have been presented to account for finite number of blades and strong curvature effects. |
| Lifting-Line Method | The propeller blades are represented by lifting lines, which have a varying circulation as a function of radius, this approach is unable to capture stall behaviour, Lerbs (1925) . |
| Lifting surface Method | The propeller blade is represented as an infinitely thin surface fitted to the blade camber line. A distribution of vorticity is applied in the spanwise and chordwise directions, Pien (1961). |
| Panel Method | Panel methods extend the lifting surface method to account for blade thickness and the hub still by representing the surface of the blade by a finite number of vortex panels, Kerwin (1987). |
| Reynolds Averaged Navier Stokes | Full 3D viscous flow field modelled using a finite volume or finite element approach to solve the averaged flow field, Adbel-Maksoud <i>et al.</i> (1998). |

The distribution of the sources may be uniform or based on radial distributions such as presented by Hough and Ordway (1965). This approach has subsequently been used by others such as Stern *et al.* (1988), Simonsen (2000), Simonsen and Stern (2005), Carrica *et al.* (2008) and Miller (2008), to represent the action of the propeller in various marine applications. Since this body force distribution is prescribed *a priori* the influence of the hull on the propeller and the rudder on the propeller is not captured by this method. More complex vortex based (lifting line) numerical methods have also been coupled with RANS simulations, Han *et al.* (2007), however, these methods are limited by potential theory that do not for example, identify propeller sectional stall or Reynold's number (scaling) effects.

Full RANS based simulation of marine propellers have been shown to be applicable for propeller design purposes, Rhee and Joshi (2005), and complete RANS simulations of a hull and propulsor, which use sliding interfaces to model the propeller rotation, have been performed, Taylor *et al.* (1998) and Lubke (2007). Mueller *et al.* (2006), used a RANS code to model the self-propelled flow around an appended Ro-Ro Twin Screw ferry travelling straight ahead. Their comparison of an explicit modelling of the full propeller through steady state and transient RANS simulation with use of a coupled blade element model of the propeller with the RANS flow over the hull showed a 90% reduction in computational effort, with only a small reduction in accuracy.

In order to reduce the significant computational cost associated with modelling the full flow field around a self propelled ship model, the RANS simulation of the flow around the manoeuvring hull form is coupled with an external Blade Element Momentum Theory (BEMT) code, Molland and Turnock (1996) developed to model propeller-rudder interaction. The implementation of this approach is described and

results are given for the prediction of the self-propulsion and manoeuvring coefficients for the KVLCC2 hull form, Van et al, (1998), Kim et al (2001).

2 Blade Element Momentum Theory

Blade element momentum theory (BEMT) is used in the design of wind turbines, Burton et al.(2001) and Mikkelsen (2003), tidal turbines , Batten *et al.* (2006) and Nicholls-Lee and Turnock (2007), and its importance for ship propeller analysis is discussed by Benini (2004). An advantage of BEMT theory over advanced methods is that it allows the lift and drag properties of the 2D sections representing the blade to be tuned to the local operating Reynolds number incorporating viscous effects such as stall or the effect of laminar separation at low Reynolds No. For turbulent flows, stall effects are difficult to capture using a RANS approach with results strongly dependent on turbulence closure models, while capturing laminar or transitional propeller sectional flow features can not be achieved using a conventional RANS turbulence closure.

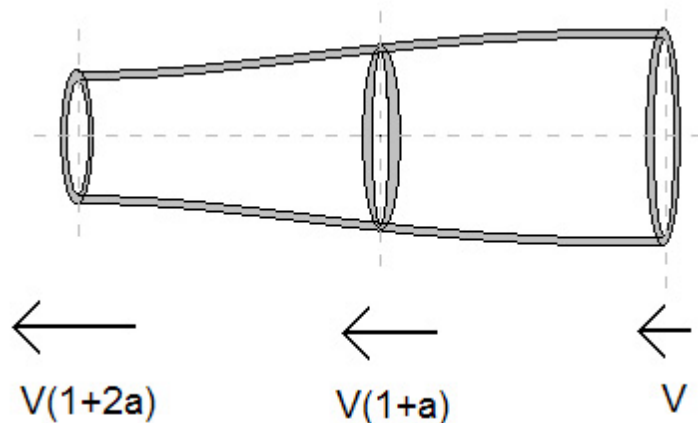


Figure 1: Actuator Disc Theory

BEMT combines the two dimensional action of the blade from blade element theory with momentum changes in the fluid from momentum theory to determine the effective angle of attack of each section and hence thrust and torque components of each section. The flow through an annulus of radius r and thickness dr at the propeller disc is considered. It can be shown that the increment of axial velocity at the disc is half that of downstream, see Figure 1, the thrust and torque acting on a length of blade dr can also be deduced. The thrust can be written as: -

$$\frac{dT}{dr} = 4\rho\pi r V^2 k a(1+a) \quad (1),$$

where a is the axial inflow factor and k is the Goldstein correction to account for the propeller having a finite number of blades, Goldstein (1929). Similarly the torque can be written as: -

$$\frac{dQ}{dr} = 4\rho\pi r^3 \Omega V k a'(1+a), \quad (2)$$

where Ω is the angular velocity of the propeller and a' is the circumferential inflow factor. The ideal efficiency η_i is found as from (1) and (2) as: -

$$\eta_i = \frac{V \frac{dT}{dr}}{\Omega \frac{dQ}{dr}} = \frac{1-a'}{1+a}. \quad (3)$$

Non dimensionalising equations (1) and (2) in terms of K_T , K_Q and J : -

$$\frac{dK_T}{dr} = \pi J^2 x k a(1+a), \quad (4)$$

$$\frac{dK_Q}{dr} = \frac{1}{2} \pi^2 J x^3 k a' (1+a). \quad (5)$$

The local lift and drag acting on the 2D blade section is given by:-

$$\frac{dL}{dr} = \frac{1}{2} \rho N C U^2 C_l(\alpha), \quad (6)$$

$$\frac{dD}{dr} = \frac{1}{2} \rho N C U^2 C_d(\alpha), \quad (7)$$

where N is the number of blades, C is the blade chord and the lift and drag coefficients C_l and C_d depend on the angle of attack α and are determined from experimental tests or numerically for the 2D section¹. The section lift and drag, see Figure 2, are resolved to give the annulus torque and thrust: -

$$\frac{dT}{dr} = \frac{dL}{dr} \cos \phi (1 - \tan \phi \tan \gamma), \quad (8)$$

$$\frac{dQ}{dr} = r \frac{dL}{dr} \cos \phi (\tan \phi + \tan \gamma). \quad (9)$$

Combining equations (8) and (9) gives the local section efficiency: -

$$\eta = \frac{\tan \psi}{\tan(\phi + \gamma)}. \quad (10)$$

¹ In this case $dC_l/d\alpha = 0.1$ $C_{d0} = 0.0107$ with section lift values calculated for zero lift incidence and drag increased as stall approached.

The motion of the fluid is modelled using the incompressible (13), isothermal Reynolds Averaged Navier Stokes (RANS) equations (14) in order to determine the Cartesian flow ($u_i = u, v, w$) and pressure (p) field of the water around the ship hull and rudder: -

$$\frac{\partial \overline{U}_i}{\partial x_i} = 0, \quad (13)$$

$$\frac{\partial \overline{U}_i}{\partial t} + \frac{\partial \overline{U}_i \overline{U}_j}{\partial x_j} = -\frac{1}{\rho} \frac{\partial \overline{P}}{\partial x_i} + \frac{\partial}{\partial x_i} \left\{ \nu \left(\frac{\partial \overline{U}_i}{\partial x_j} + \frac{\partial \overline{U}_j}{\partial x_i} \right) \right\} - \frac{\partial \overline{u'_i u'_j}}{\partial x_i} + f_i. \quad (14)$$

The RANS equations are implemented in the commercial CFD code ANSYS CFX 11 (CFX), ANSYS CFX (2006). The governing equations are discretised using the finite volume method. The high-resolution advection scheme was applied for the results presented which varies between first and second order accuracy depending on spatial gradient. For a scalar quantity ϕ the advection scheme is written in the form

$$\phi_{ip} = \phi_{up} + b \nabla \phi \cdot R, \quad (16)$$

where ϕ_{ip} is the value at the integration point, ϕ_{up} is the value at the upwind node and R is the vector from the upwind node to the integration point. The model reverts to first order when $b=0$ and is a second order upwind biased scheme for $b=1$. The high resolution scheme calculates b using a similar approach to that of Barth and Jeperson (1989), which aims to maintain b locally to be as close to one as possible without introducing local oscillations. Collocated (non-staggered) grids are used for all transport equations, and pressure velocity coupling is achieved using an interpolation scheme based on that proposed by Rhie and Chow (1982). Gradients are computed at

integration points using tri-linear shape functions defined in ANSYS CFX (2006). The linear set of equations that arise by applying the Finite Volume Method to all elements in the domain are discrete conservation equations. The system of equations is solved using a coupled solver and a multigrid approach.

The Shear Stress Transport (SST), Menter (1994), turbulence closure model was selected for this study since previous investigations have shown that it is better able to replicate the flow around ship hull forms than either zero equation models or the $k-\epsilon$ model, notably in capturing hooks in the wake contours at the propeller plane, Larsson *et al.* (2003).

5 Coupled RANS BEMT Method

Within the RANS mesh the propeller is represented as a cylindrical sub-domain with a diameter, D , equal to that of the propeller and a length of $0.15D$. The sub domain is divided into a series of ten annuli corresponding to ten radial slices (dr) along the blade. The appropriate momentum source terms from (4) and (5) are then applied over the sub-domain in cylindrical co-ordinates to represent the axial and tangential influence of the propeller.

The following procedure is adopted in order to calculate the propeller performance and replicate it in the RANS simulations.

1. An initial converged stage of the RANS simulation (RMS Residuals $< 1E^{-5}$) of flow past the hull is performed, with the propeller domain body force terms set to zero.

2. The local nominal wake fraction, w_T' , is determined for each annulus by calculating the average circumferential mean velocity at the corresponding annuli.

$$w_T' = \frac{1}{2\pi r} \int_0^{2\pi} \left(1 - \frac{U}{V_a}\right) r d\theta, \quad (15)$$

where U is the axial velocity at a given r and θ . This captures the influence of the hull and rudder on the flow through and across the propeller disc. This calculation is written as a user specified Fortran module that exports the set of local axial wake fractions to the BEMT code.

3. The BEMT code iterates to find the thrust (dK_T) and torque (dK_Q) for the ten annuli based on ship speed, the local nominal wake fraction and the propeller rpm and applying (4) through (10). A converged solution is deemed to have occurred when the difference in α is less than 1% . This phase of analysis adds a negligible overhead to the overall computational cost.
4. The local thrust and torque derived by the BEMT code are assumed to act uniformly over the annulus corresponding to each radial slice. The thrust is converted to axial momentum sources (momentum/time) distributed over the annuli by dividing the force by the volume of annuli. The torque is converted to tangential momentum sources by dividing the torque by the average radius of the annulus and the volume of the annulus.
5. These momentum sources are then returned to the RANS solver by the Fortran Module which distributes them equally over the cell within the axial length of the propeller disc.
6. The RANS simulation is then restarted from the naked hull solution but now with the additional momentum sources. The final solution is assumed to have

converged when the root mean square residual is less than $1E^{-5}$. Typically the computational cost of this second phase of the RANS simulation adds a further 30%.

It should be noted that the procedure discussed above calculates the propeller inflow conditions based on the nominal wake field, i.e the wake field without the presence of the propeller. In practice when a propeller is operating in the wake of a ship the total velocity field is the sum of the nominal wake field, the propeller induced velocities and interaction velocities due to the complex interaction between the hull and propeller, Carlton (2007). Thus ideally the input to the propeller model would be the effective wake field which is the sum of nominal wake and induced velocities. It is possible to find the effective wake field by repeating the process from steps 2 through 6 to find the total velocity field then subtracting the propeller induced velocities calculated from the BEMT code, see Phillips *et al.* (2008). For the particular geometry investigated only very small changes occur and this additional iterative loop was not included.

6 Evaluation of the coupled BEMT-RANS using the KVLCC2 hull

The KRISO Very Large Crude Carrier 2 (KVLCC2), see Figure 3 and Table 2 for hull particulars, is a well documented experimental test case for CFD code evaluation, Larsson *et al.* (2003), Hino (2005) and Stern and Agdrup (2008). The KVLCC2 was designed by the Korean Institute of Ships and Ocean Engineering (KRISO now MOERI) and is representative of full bodied ships ($C_B = 0.81$) single screw tankers. The hull form incorporates a bulbous bow and a transom stern.

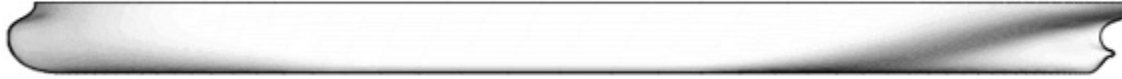


Figure 3: KVLCC2 Hull Form

Table 2: Principal Dimensions of the KVLCC2 Model and Propeller

| Dimension | Full-Scale | Model-Scale |
|----------------|------------|-------------|
| Scale | 1.00 | 58.000 |
| $L_{pp}(m)$ | 320.0 | 5.5172 |
| $B_{wl}(m)$ | 58.0 | 1.0000 |
| D (m) | 30.0 | 0.5172 |
| T (m) | 20.8 | 0.3586 |
| $\nabla (m^3)$ | 312622 | 1.6023 |
| Type | FP | FP |
| No. Blades | 4 | 4 |
| D(m) | 9.86 | 0.170 |
| P/D(0.7R) | 0.721 | 0.721 |
| A_e/A_o | 0.431 | 0.431 |
| Rotation | Right Hand | Right Hand |
| Hub Ratio | 0.155 | 0.155 |

As part of the SIMMAN 2008 Workshop on Verification and Validation of Ship Manoeuvring Simulation Methods model tests were performed at the MOERI test tank (200m long x 16m wide x 7 deep) on a 1/58.0 scale self propelled model, at a range of speeds, drift angles and rudder angles. The model was fitted with a propeller and a semi-balanced rudder based on a NACA0018 section with an area of $0.0654m^2$ and a geometric aspect ratio of 1.55.

A series of static drift, static rudder, pure sway planar motion mechanism (PMM) tests and pure yaw PMM tests were performed with the propeller operating at the ship propulsion point (515 rpm) at a model speed of 1.047m/s corresponding to 15.5 knots full scale ($Fn=0.14$ and model scale $Rn = 4.6 \times 10^6$).

Figure 4 demonstrates the application of the BEMT when predicting the given open water performance of the model propeller, provided by MOERI with the

performance predicted by BEMT. For the effective advance speed of interest for this work (nominal $J = 0.35$) the agreement for K_T and K_Q was excellent, with a difference of less than 1%. It should be noted that the propeller diameter based Reynolds Number ($Rn = VD/\nu$) is 150,000 and as such a full turbulent RANS propeller simulation would not be appropriate. Table 3 summarises the computational parameters adopted.

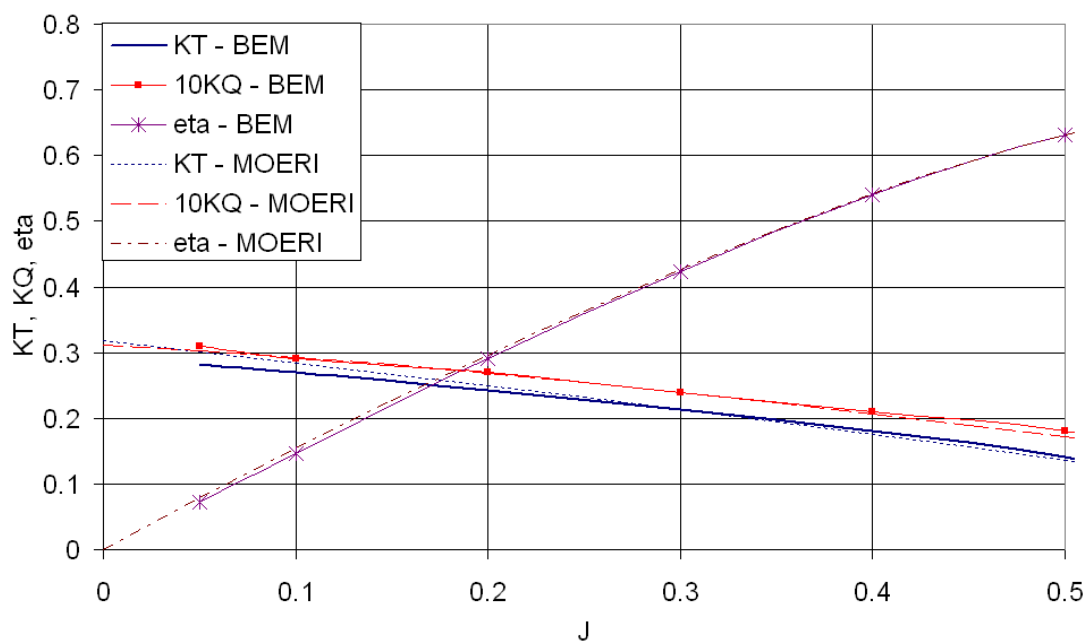


Figure 4: Comparison of Propeller Characteristics in Open Water. Experimental data made available as part of the SIMMAN workshop, Stern F., Agdrup K., editors 2008

Table 3: Computational model

| Parameter | Setting |
|---------------------|---|
| Computing | 64-bit desktop pc 4GB of RAM |
| Mesh Type | Unstructured –hybrid (tetrahedra/prism) |
| Turbulence Model | Shear Stress Transport [40] |
| Advection Scheme | CFX High Resolution |
| Convergence Control | RMS residual $<10^{-5}$ |

6.1 Mesh Definition

A hybrid finite volume unstructured mesh was built with the meshing tool ANSYS ICEM V11, using tetrahedra in the far field and inflated prisms elements around the hull with a first element thickness equating to a $y^+ = 30$, with 10 to 15 elements used to capture the boundary layer of both hull and rudder. Separate meshes were produced for each rudder angle using a representation of the horn rudder with sealed gaps between the movable and fixed part of the rudder, see Figure 5.

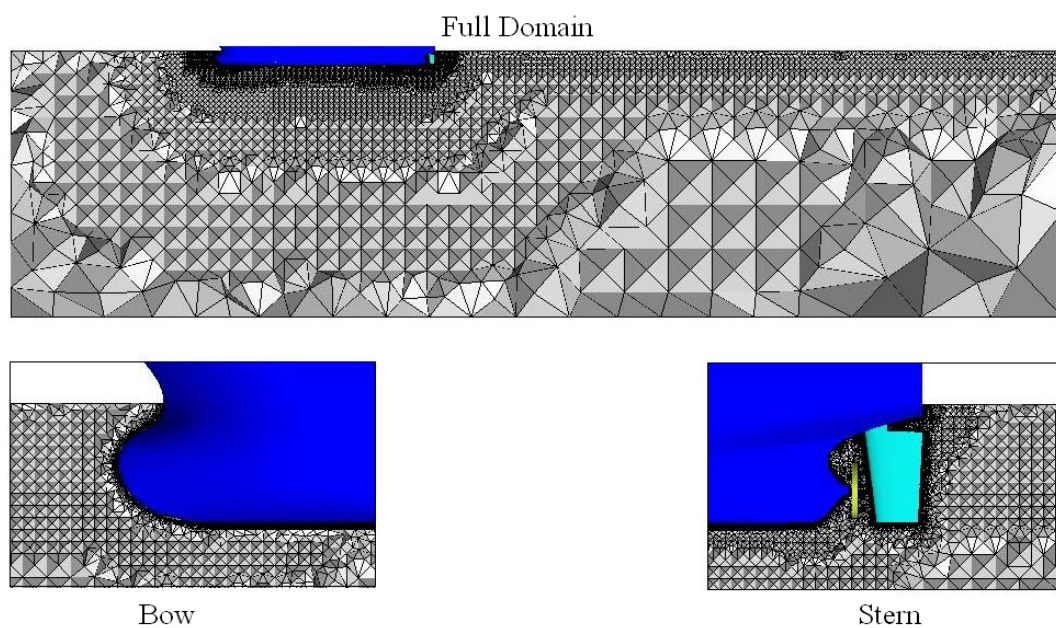


Figure 5: Mesh cut plane through longitudinal centreline of ship

6.2 Boundary Conditions

The solution of the RANS equations requires a series of appropriate boundary conditions to be defined. The hull is modelled using a no-slip wall condition. Based on previous experience a Dirichlet inlet condition, one body length upstream of the hull is defined where the inlet velocity and turbulence are prescribed explicitly. The model scale velocity is replicated in the CFD analyses; and inlet turbulence is set at the default value of 5%. A mass flow outlet is positioned 3 body lengths downstream of the hull.

The influence of tank size on hydrodynamic derivatives determined from CFD simulations has been demonstrated by Brogali *et al.* (2006), thus to replicate the test conditions free slip wall conditions are placed at the locations of the floor and sides of the tank (16m wide x 7m deep) to enable direct comparison with the experimental results without having to account for blockage effects ($D_T/T = 19.5$ and $L/B_T = 0.345$). The influence of free surface is not included in these simulations due to the increase in computational cost, and the free surface is modelled with a symmetry plane. The Froude number is sufficiently low, $Fn=0.14$, that this is not expected to have a large effect.

6.3 Mesh Sensitivity

An uncertainty assessment has been performed based on the methodology presented by Stern *et al.* (1999). While not directly applicable to a hybrid mesh, it is assumed to be a suitable approach when using a hybrid meshing strategy where the mesh in the boundary layer is systematically refined. Table 4 shows the results of mesh sensitivity study for the self propelled case with the rudder at 10° using a refinement ratio of $r_k = \sqrt{2}$ with the finest mesh having 2.1×10^6 elements, within the boundary layer modification of the first later thickness modified the y_+ value from 30 on the finest mesh to 60 on the coarsest.

Computational uncertainty was found to be 2-3% for side force and yaw moment but much larger at 15% for resistance. Previous CFD workshops highlight the difficulties in accurate prediction of straight line resistance, with large uncertainty and comparison errors common between calculated and experimental drag unless significantly larger meshes (10M+ elements) are used Hino *et al.* (2005). Thus a mesh density of 2M cells proves inadequate to achieve a fully mesh independent solution capturing all aspects for self propulsion and propeller design calculations.

Nonetheless, a good level of understanding of the global forces and moments required for manoeuvring coefficients can be obtained with this level of mesh resolution.

Table 4: Uncertainty Analysis – Self Propulsion – Rudder at 10°

| | Exp. (D) | Fine (S _G) | Medium | Coarse | U _G (%S _G) | E (%D) | U _v (%D) |
|------------------------------------|-------------|---------------------------|--------|--------|--------------------------------------|--------|------------------------|
| Longitudinal Force X(N) | -11.05 | -11.74 | -12.60 | -13.82 | 17.50 | -6.28 | 18.77 |
| Transverse Force, Y (N) | 6.79 | 7.6 | 7.51 | 7.33 | 1.35 | -11.89 | 2.92 |
| Yaw Moment, N (Nm) | -19.47 | -18.75 | -18.70 | -18.35 | 0.49 | 3.70 | 2.54 |
| Thrust, T (N) | 10.46 | 12.53 | 12.37 | 12.08 | 1.57 | -19.79 | 3.13 |
| Rudder X Force, R _x (N) | -2.02 | -1.83 | -1.89 | -1.94 | - | 9.39 | - |
| Rudder Y Force, R _y (N) | 4.32 | 4.94 | 4.99 | 4.88 | - | -14.49 | - |

7 Results

7.1 Hull-Propeller-Rudder Interaction

Figure 6 shows the spanwise variation of dK_T and dK_Q along the blade due to the local nominal wake fraction (w_T'), the average nominal wake fraction (w_T) over the propeller disc was calculated at 0.467 compared with 0.443 derived experimentally.

The momentum terms used to replicate the action of the propeller in the RANS simulation lead to a thrust deduction factor, $t=(T-R)/T$, of 0.236 compared to the value of 0.190 derived experimentally. Figures 7 and 8 illustrate the influence of the propeller on the hull surface pressure and skin friction distribution respectively, for the without rudder case. Note, the propeller model introduces asymmetry in the flow by replicating the swirl effect of the propeller, consequently the illustrated

starboard view shown differs slightly to the port side of the vessel. The local acceleration of the flow due to the propeller leads to a reduction in local pressure coefficient, $C_p=(P-P_0)/(1/2\rho U_0^2)$, and an increase in the skin friction coefficient $C_f=\tau_w/(1/2\rho U_0^2)$. These effects are concentrated at the stern of the vessel, diminishing as the parallel mid-body is approached.

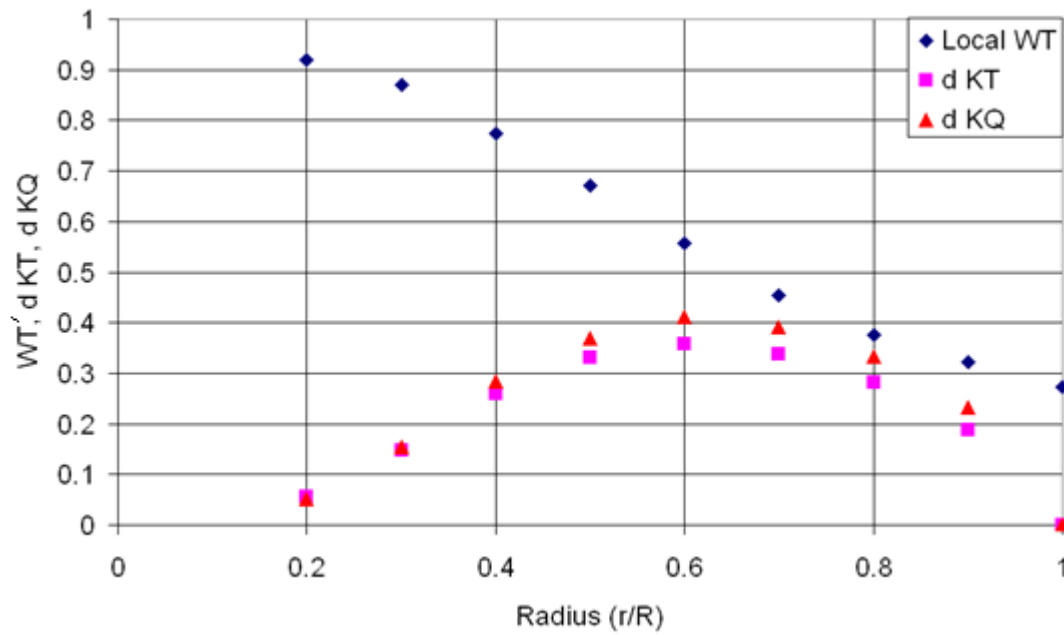


Figure 6: Variation in nominal wT , dK_T and dK_Q along blade radius

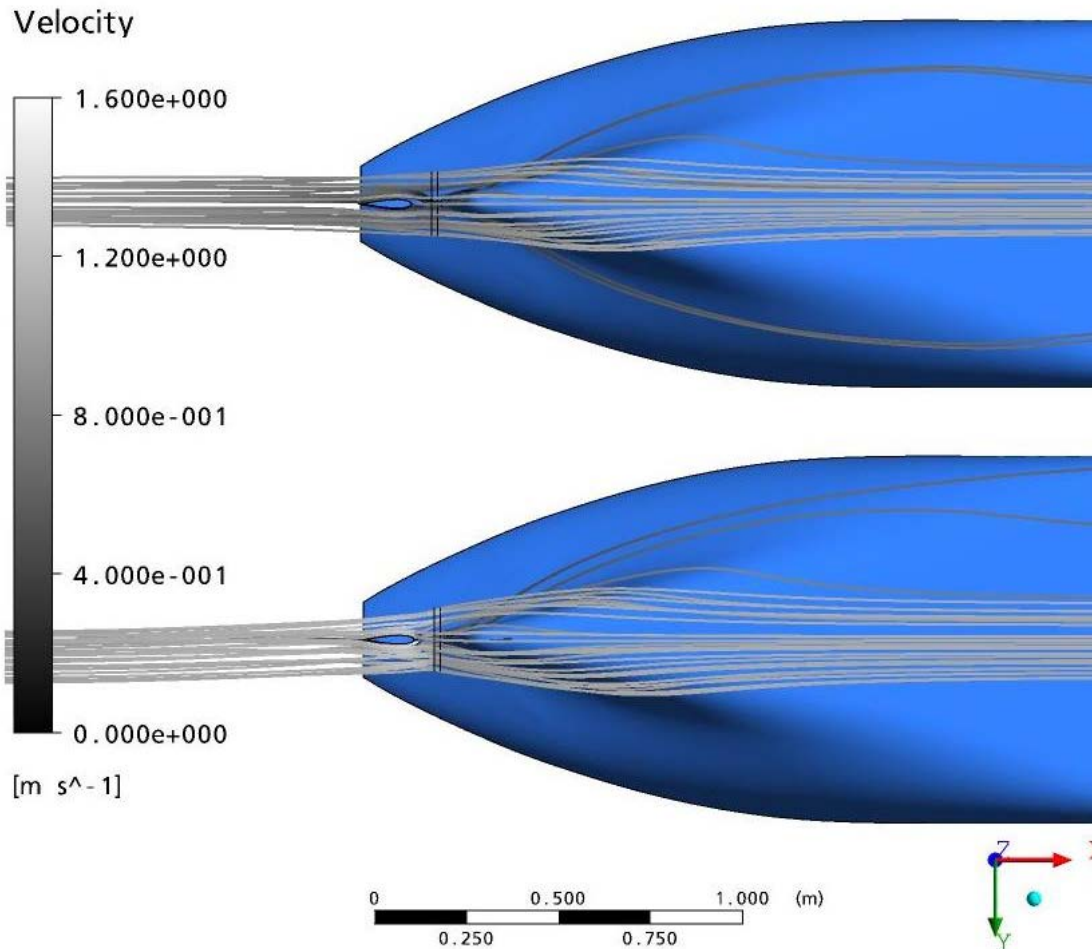


Figure 7: Comparison of streamlines passing through the propeller disc for the appended hull, no propeller model (top), propeller model on (bottom)

The action of the propeller accelerates the flow and induces a swirl component. This travels downstream where it flows onto the rudder significantly changing the flow around the rudder without the propeller, see Figure 9. The net result of the propeller action is an increase in the velocity and an effective angle of incidence, leading to an increase in rudder drag and the production of rudder lift, with the rudder at zero incidence.

The presence of the rudder modifies the flow upstream into the propeller influencing the performance of the propeller, see Table 5. Blockage from the rudder reduces the flow velocity into the propeller, increasing the nominal mean wake fraction, w_T by 0.018, resulting in an increase in the thrust and torque coefficients.

The change in the local wake fraction and the drag from the rudder modifies the rpm required at the model propulsion point from 552 rpm to 542rpm. Comparing the thrust coefficient with and without the action of the propeller results in a $\Delta K_T = 0.07$ at a rudder separation $X/D = 0.28$. This compares well with the wind tunnel experiments by Molland and Turnock (2007) which derived a $\Delta K_T = 0.058$ at a $X/D = 0.3$ for a similar rudder and propeller thrust loading.

7.2 Global Forces

The global loads acting on the vessel are non-dimensionalised by the length of the vehicle (L) the velocity of the vehicle (V) and the density of the fluid (ρ), a prime symbol is used to signify the non dimensional form for example: -

$$v' = \frac{v}{V}, \quad Y' = \frac{Y}{1/2 \rho L^2 V^2}, \quad N' = \frac{N}{1/2 \rho L^3 V^2} \quad (15)$$

The axis system is described in Figure 10. The matching set of experiments were performed with the vessel restrained in roll but free to heave and pitch, however, to reduce simulation time the CFD simulations have assumed the vessel is fixed in heave and pitch at the quoted mean draught and level keel. For the zero drift, zero rudder angle case the force in the z direction was 253N downwards, which corresponds to a sinkage of 5.1mm equating to 1% of the draft.

Figures 11 illustrate the variation of global forces with variation in drift angle. The influence of drift angle on global loads is well captured even at larger amplitude drift angles outside the linear region.

Prediction of the rudder forces is dependent on the rudder inflow conditions which are dominated by the action of the hull and the propeller. Thus to accurately capture the rudder forces the flow in the stern of the vessel needs to be captured with

a high level of accuracy, to ensure the correct flow into the propeller and then across the rudder. Small over predictions in the thrust generated by the propeller will lead to an increased inflow velocity which will then cause an over prediction of rudder force. This is seen in Figure 12, where the predicted propeller thrust is approximately 20% higher than the experimental result, leading to over prediction of the global side force and yawing moment which are dominated by the rudder loads. It should be noted that only 13500 surface mesh elements were used to define the rudder, surrounded by a mesh of the order 200,000 cells in the vicinity of the rudder. Work by Date and Turnock (2002) indicate values of 5-20M cells are required to fully resolve the rudder force.

These simulations provide good initial estimates of the manoeuvring coefficients for the appended KVLCC2 hullform. The results would benefit from finer mesh resolution in the boundary layer region, resolving into the viscous sub layer would remove uncertainty resulting in using wall functions, finer resolution in the region of the bilge vortices would improve the both the prediction of the hull surface pressure and prediction of the propeller inflow, while further mesh density around the rudder and rudder tip vortex would improve prediction of the rudder forces.

The coupled RANS-BEMT approach circumferentially averages propeller inflow for a series of annuli. This fails to capture the circumferential variation in blade loading and consequently propeller side force. A more complete approach would be to subdivide the propeller disc into a series of discrete zones in both the radial and circumferential direction. Such an approach would add negligible computational cost but provide a more complete representation of the influence of the propeller within the RANS simulation, Phillips *et al.* (2008).

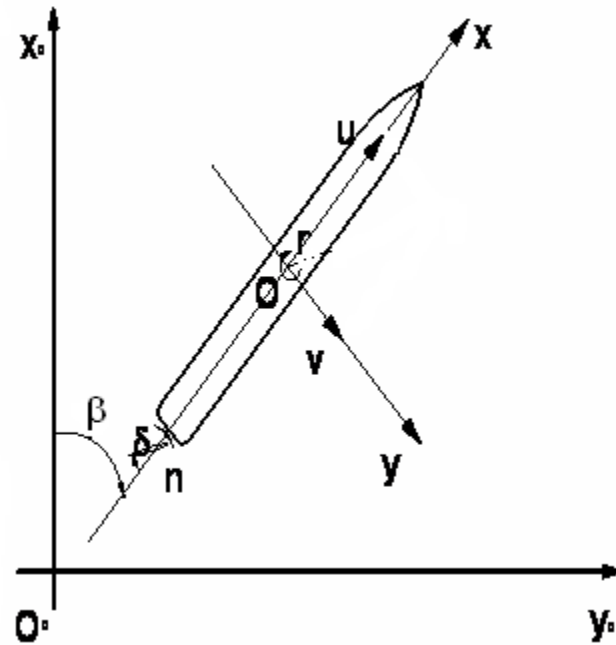


Figure 8: Axis System

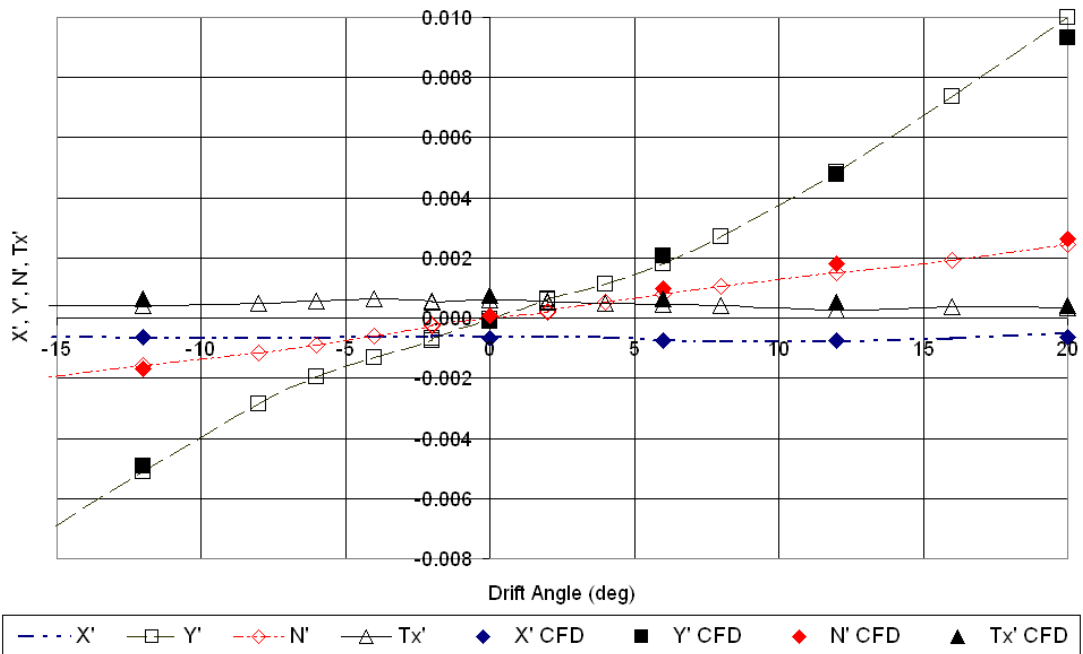


Figure 9: Influence of Drift Angle on Force Coefficients at a Model speed of 1.047m/s Experimental data made available as part of the SIMMAN workshop, Stern F., Agdrup K., editors 2008

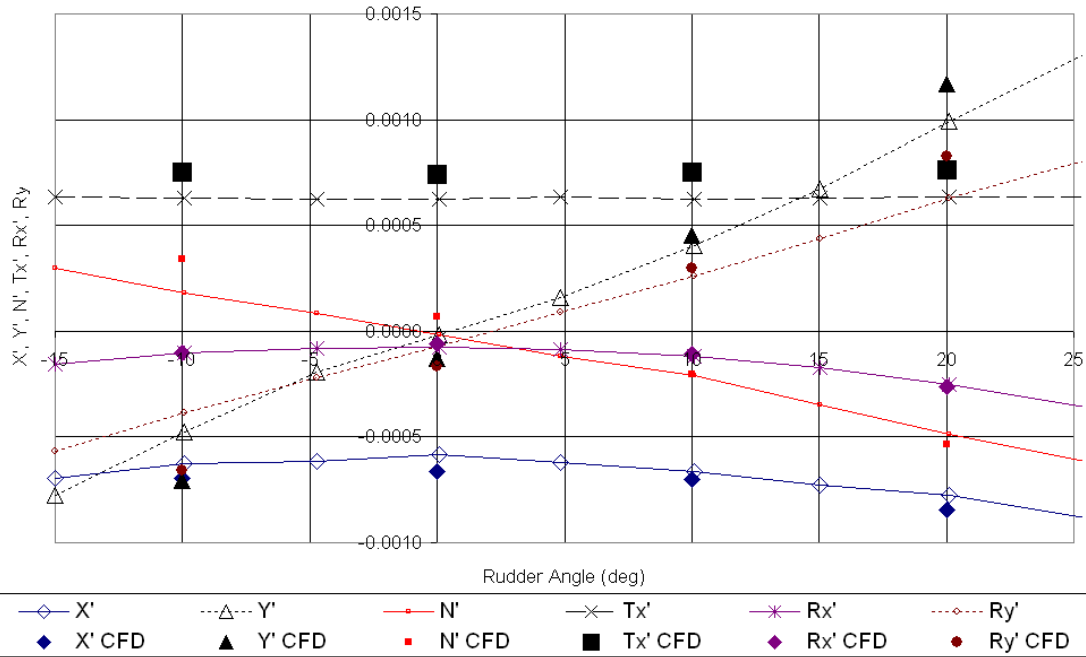


Figure 10: Influence of Rudder Angle on Force Coefficients at a Model speed of 1.047m/s. Experimental data made available as part of the SIMMAN workshop, Stern F., Agdrup K., editors 2008

8 Conclusions

A method of coupling a Blade Element Momentum Theory code for marine propellers with the commercial RANS code ANSYS CFX is presented. As a demonstration of the effectiveness of the approach a coupled CFD-BEMT simulation of the flow around the model scale KVLCC2 tanker was able to predict the global forces and moments acting on a vessel undergoing self propelled steady state manoeuvres with good agreement. This was with a computational uncertainty of 2-3% for manoeuvring side force and yaw moment. The method captures the changes in propulsive force associated with the downstream rudder and increase in rudder sideforce associated with the acceleration of the propeller race. It is estimated that computational cost of running a propeller model based approach is 1/10th of the cost of considering the full transient flow field with an unsteady BEMT. A one to two

order of magnitude reduction in timestep is likely to be required to fully model the propeller in RANS, Mueller et al, (2006).

References

- Abdel-Maksoud, M., Menter F., Wuttke, H., 1998. Viscous flow simulations for conventional and high-skew marine propellers. *Ship Technology Research*, vol. 45.
- ANSYS CFX. ANSYS CFX, Release 11.0. ANSYS, 2006.
- Barth, T.J., and Jespersen, D.C, 1989. The Design and Application of Upwind Schemes on Unstructured Meshes, AIAA Paper 89-0366.
- Batten, W.M.J., Bahaj, A.S., Molland, A.F., Chaplin, J.R., 2006. Hydrodynamics of marine current turbines. *Renewable Energy*, vol. 31, pp249–256.
- Benini, E., 2004. Significance of blade element theory in performance prediction of marine propellers. *Journal of Ocean Engineering*, vol.31,pp957–974.
- Bertram, V., 2000. *Practical Ship Hydrodynamics*. Butterworth Heinemann.
- Breslin, J.P., Anderson, P., 1994. *Hydrodynamics of ship propellers*. Cambridge University Press., 1994.
- Brogali, R., Muscari, R., Di Mascio A., 2006. Numerical analysis of blockage effects in pmm tests. In Proc.26th Symposium on Naval Hydrodynamics Rome, Italy, 17-22 September.
- Burton, T., Sharpe, D., Jenkins, N., Bossanyi., E., 2001 *Wind Energy : Handbook*. Chichester Wiley.
- Carlton, J., 2007, *Marine Propellers and Propulsion*, Elsevier, Oxford, 2nd Edition.
- Carrica, P.M., Ismail F., Hyman, M., Bushan, S., F. Stern, F., 2008. Turn and zigzag manoeuvres of a surface combatant using a URANS approach with dynamic

- overset grids. In SIMMAN 2008 Workshop on Verification and Validation of Ship Manoeuvring Simulation Methods, Copenhagen April 14th-16th.
- Comstock, J.P., (ed.) 1967, Principles of Naval Architecture, The Society of naval Architects and Marine Engineers, New York.
- Date, J.C., Turnock, S.R., 2002. Computational Evaluation of the Periodic Performance of a NACA 0012 Fitted With a Gurney Flap, Journal of Fluids Engineering, vol. 124, pp227-234.
- Froude, R.E., 1889. On the part played in propulsion by differences of fluid pressure. Transactions of the Royal Institute of Naval Architects.
- Froude, R.E., 1911. The acceleration in front of a propeller. Transactions of the Royal Institute of Naval Architects.
- Froude, W., 1878. On the elementary relation between pitch, slip and propulsive efficiency. Transactions of the Royal Institute of Naval Architects.
- Goldstein, S., 1929. On the vortex theory of screw propellers. In proceedings of the Royal Society.
- Han, K-J., Larsson, L., and Regenstrom, B.,. A RANS study on the interaction between a propeller and a rudder in open water. In 10th Numerical Towing Tank Symposium, Hamburg, 2007.
- Hino, T., editor 2005. CFD Workshop Tokoyo. National Maritime Research Institute.
- Hough, G.R., Ordway, DE., 1965. The generalised actuator disc, Developments in Theoretical and Applied Mechanics, vol. 2, pp317–336.
- Kerwin, J.E., Kinnas, S.A. Lee, J., Shih, W., 1987. A surface panel method for the hydrodynamic analysis of ducted propellers. Transactions of SNAME vol.95.
- Kim, W.J., Van, S.H. and Kim, D.H., 2001, Measurement of flows around modern commercial ship models, Exp. in Fluids, Vol. 31, pp 567-578.

- Larsson, L., Stern, F., Bertram, V., 2003 Benchmarking of computational fluid dynamics for ship flows: The Gothenburg 2000 workshop. *Journal of Ship Research*, vol.47, pp81-100
- Lerbs, H.W., 1925. Moderately loaded propellers with a finite number of blades and an arbitrary distribution of circulation. *Transaction of SNAME*, vol. 60.
- Lubke, L., 2007. Investigation of a semi-balanced rudder. In 10th Numerical Towing Tank Symposium, Hamburg, Germany 23-25 September.
- Menter, F.R., 1994. Two-equation eddy-viscosity turbulence models for engineering applications. *AIAA Journal*, vol.32(8),pp1598 – 1605.
- Mikkelsen, R., 2003. Actuator Disc Methods Applied to Wind Turbines. PhD thesis, Department of Mechanical Engineering Technical University of Denmark.
- Miller, R.W., 2008. PMM calculations for the bare and appended DTMB 5415 using the RANS solver CFDSHIP-IOWA. In SIMMAN 2008 Workshop on Verification and Validation of Ship Manoeuvring Simulation Methods, Copenhagen April 14th-16th.
- Molland, A.F., Turnock, S.R., 1996. A compact computational method for predicting forces on a rudder in a propeller slipstream. *Transactions of RINA*, vol. 138, pp 59–71.
- Molland, A.F., and Turnock, S.R., 2007. *Marine Rudders and Control Surfaces*. Butterworth-Heinemann.
- Mueller, S.B., Steden, M., Neugebauer, J., El-Haddad, M.F., Abdel Maksaud, M., 2006. Comparing a propeller model with a rotating propeller in a CFD-simulation of the viscous flow around a ship. In 9th Numerical Towing Tank Symposium, le Croisic, France, 1-3 October.

- Nicholls-Lee, R., Turnock, S.R., 2007. Enhancing performance of a horizontal axis tidal turbine using adaptive blades. In OCEANS 2007, Aberdeen, Scotland 18th-21st June.
- O'Brian, T.P., 1969. The Design of Marine Screw Propellers. Hutchinson Scientific and Technical, Third Impression Edition.
- Pien, P.C., 1961. The calculation of marine propellers based on lifting surface theory. Journal of Ship Research, vol.5.
- Phillips, A.B., Turnock, S.R. and Furlong, M. 2008. Comparisons of CFD simulations and in-service data for the self propelled performance of an Autonomous Underwater Vehicle. In, *27th Symposium of Naval Hydrodynamics, Seoul, Korea, 5-10 Oct 2008.* Seoul, Korea, Office of Naval Research, 15pp.
- Rankine, W.J.M., 1865. On the mechanical principles of the action of propellers. Transactions of Royal Institute of Naval Architects.
- Rawson, K.J., Tupper, E.C., 2001. Basic Ship Theory Fifth Edition. Butterworth Heinemann
- Rhee, S.H., Joshi, S., 2005. Computational validation for flow around a marine propeller using unstructured mesh based Navier-Stokes solver. JSME International Journal Series B, vol. 48, No. 3, pp.562– 570.
- Rhie, C.M. and Chow, W.L.,1982. A Numerical Study of the Turbulent Flow Past an Isolated Airfoil with Trailing Edge Separation. AIAA Paper 82-0998., 1982
- Schetz, J.A., Favin S., 1977. Numerical solution for the near wake of a body with a propeller. Journal of Hydronautics, vol 11, pp136–141.
- Simonsen, C. D., 2000. Rudder, Propeller and Hull Interaction br RANS. PhD thesis, Department of Naval Architecture and Offshore Engineering, Technical University of Denmark.

- Simonsen C.D., Stern, F., 2005. RANS manoeuvring simulation of Esso Osaka with rudder and a body-force propeller. *Journal of Ship Research*, vol. 49, pp98–120.
- Stern, F., Kim, H.T., Patel, N.M., Chen H.C., 1988. A viscous-flow approach to the computation of propeller-hull interaction. *Journal of Ship Research*, vol. 32, pp246–262.
- Stern, F., Wilson, R.V., Coleman, H.W., Paterson, E.G., 1999. Verification and validation of CFD simulations. Technical Report IIHR Report No. 407, Iowa Institute of Hydraulic Research, September.
- Stern F., Agdrup K., eds. 2008. SIMMAN 2008 workshop on verification and validation of ship manoeuvring simulation methods. In *Draft Workshop Proceedings*.
- Turnock, S.R., 1993. Prediction of ship rudder-propeller interaction using parallel computations and wind tunnel measurements. University of Southampton, Ship Science, PhD Thesis, 358pp.
- Van, S.H., Kim, W.J., Yim, G.T., Kim, D.H., and Lee, C.J., 1998, Experimental Investigation of the Flow Characteristics Around Practical Hull Forms, *Proceedings 3rd Osaka Colloquium on Advanced CFD Applications to Ship Flow and Hull Form Design*, Osaka, Japan